Testing of short−wave irradiance retrieval algorithms under cloudy conditions[1]

ØYSTEIN GODØY[2] AND STEINAR EASTWOOD

Norwegian Meteorological Institute[3]

(24 June 2002)

1 Introduction

The Norwegian Meteorological Institute (DNMI) is part of the EUMETSAT Satellite Application Facility (SAF) for Ocean and Sea Ice (OSI). DNMI shall, among other tasks, develop a system for estimation of the downward surface solar irradiance (SSI) using polar orbiting satellites (NOAA POES and EUMETSAT EPS). In the low and mid latitude part Météo France are developing algorithms for the future EUMETSAT geostationary satellite Meteosat Second Generation (MSG) using data from NOAA GOES. The output radiative flux to be delivered by the High Latitude SAF (HL) is daily estimates of surface solar irradiance at 10km resolution north of 50°N and potentially south of 50°S.

This document is part of a series of reports addresses the problems that has to be solved when operational narrowband AVHRR radiance measurements are used to estimate the short−wave irradiance (flux) at the ground. Throughout this document the downward surface short−wave flux will be denoted as SSI.

SSI is usually defined as radiation in the 0.3−4.0 μm band. Operational weather satellites usually measures radiance in narrow bands within this broadband while surface stations measuring the short−wave flux have pyranometers observing broadband values, usually in the 0.3−2.8 μm band, thus there is a slight error source for validation, but other sources are supposed to be larger.

2 Method

The solar irradiance at the surface under cloudy conditions is (using the same terminology as Brisson et al., 1999) a function of the solar irradiance at the top of the atmosphere, the atmospheric transmittance (T_a) which is consistent with the clear sky atmospheric transmittance and the combined effects of clouds through a cloud factor (T_{cl}):

1 This report is published in the Research Note series at the Norwegian Meteorological Institute: DNMI Research Note No. 69, ISSN 0332−9879, Norwegian Meteorological Institute, 2002, 20pp.

2 email: o.godoy@met.no

3 P.O.BOX 43, Blindern, N−0313 OSLO, NORWAY

$$E = S' \mu_0 T_a T_{cl}$$

$$S' = \frac{S_0}{\rho^2}$$

$$\mu_0 = \cos\sigma$$

where σ is the solar zenith angle, S_0 is the solar constant (1358 W/m^2 when band weighted). ρ^2 is a correction factor for the varying distance between the earth and the Sun and is given below. The annual cycle in the extraterrestrial solar irradiance is approximately ±3% about the mean due to a variation in the distance between the earth and the Sun. This variation can be defined in different ways, the implementation at DNMI follows the specification of Paltridge and Platt (1976).

$$\rho^2 = \frac{1}{1.00011 + 0.034221\cos\theta + 0.001280\sin\theta + 0.000719\cos 2\theta + 0.000077\sin 2\theta}$$

where

$$\rho^2 = \frac{D^{SE}}{\overline{D^{SE}}} \quad \text{and} \quad \theta = \frac{2\pi d_n}{365} = 0.9863 d_n$$

D^{SE} is the actual distance between the Sun and the Earth and $\overline{D^{SE}}$ is the mean distance (referring to 1*AU*). d_n is the Julian Day of the year starting at 0 on January 1 and ending at 364 on December 31. In the equation for θ above the first statement produces output in radians and the last in degrees.

The clear sky transmittance (T_a) is not dependent on the satellite observation, it is merely a function of solar zenith angle and atmospheric load of water vapour, ozone, and aerosol and the surface albedo. The clear sky parameterization used in this study is described in Darnell et al. (1988) and Darnell et al. (1992) and evaluated in Godøy (2000). The atmospheric transmittance is estimated as a function of absorption in water vapour, ozone, oxygen, and carbon dioxide, scattering by aerosols and Rayleigh scattering. The atmospheric back−scatter is parameterized by the surface pressure and albedo:

$$T_a = e^{-\tau}(1 + 0.065\, p_s A_s)$$

$$\tau = \tau_0 \left(\frac{1}{\mu_0}\right)^N, \text{where } N = 1.1 - 2\tau_0$$

$$\tau_0 = \tau_{O3} + \tau_{H2O} + \tau_{CO2} + \tau_R + \tau_a$$

$$\tau_{O3} = 0.038 U_{O3}^{0.44}$$

$$\tau_{H2O} = 0.104 U_{H2O}^{0.3}$$

$$\tau_{O2} = 0.0076 p_s^{0.29}$$

$$\tau_R = 0.038 p_s$$

$$\tau_a = 0.007 + 0.009 U_{H2O}$$

In the equations above, τ represents the optical depth due to various absorbers, μ_0 is as

before the cosine of the solar zenith angle, p_s is the nominal surface atmospheric pressure in atmospheres and U is the atmospheric load (in cm) of various constituents.

The cloud factor (T_{cl}) is a function of the cloud albedo and requires several processing steps to be determined. Adapting the procedure described by NOAA/NOAASIS and described by Rao and Chen at the NOAASIS home page[4], the digital counts are converted to scaled radiance or often called albedo using a standard linear relationship for the visible channels (NOAA−14 and prior, split−gain for successors). Using the nomenclature of NOAA the "albedo" or better − "reflectance factor" or "scaled radiance" is given as:

$$A = SC_{10} + I$$

where C_{10} is the 10−bit count value, S and I are the slope and intercept. The basic processing of AVHRR data at DNMI provides A.

The equation above gives the reflectance factor for overhead sun. In this experiment, the reflectance factor is converted to a pseudo bi−directional reflectance by division with the cosine of the solar zenith angle.

$$r = \frac{\rho^2 A}{\cos\theta_0}$$

r in the range 0−100 is input to the SSI computations, but is transformed to the range 0−1 before it is used to estimate the cloud transmissivity. Before the satellite observation can be used for SSI estimation it has to be converted to a directional independent albedo measure. This is done by first performing a narrowband to broadband correction (Godøy and Eastwood, 2002, Hucek and Jacobowitz, 1995), and then an anisotropy correction (Godøy, 2002, Manalo−Smith et al., 1998).

It is well known that the visible channels of the AVHRR instrument is subject to degradation after launched into space. The corrections proposed by Rao and Chen (1996, 1999) is used on the NOAA−14 data used in this study, no correction was applied to NOAA−12 and NOAA−15 data.

The main topic of this report is to compare methods for determination of T_{cl} the cloud factor.

3 Algorithms

In this chapter the equations used for cloud transmittance estimation and clear sky transmittance parameterization are presented. First the cloud parameterizations are presented as these are the ones to be tested, then the clear sky parameterizations are presented as these are necessary for the cloud parameterization. They describe the effects of various gases in the atmosphere on the transmittance.

4 http://noaasis.noaa.gov/NOAASIS/ml/calibration.html

3.1 Cloud transmittance

3.1.1 Introduction

Generally the cloud transmittance is related to the cloud albedo through the relationship:

$$a_c + T_c + A_c = 1$$

where a_c represents cloud absorption, T_c represents cloud transmission and A_c represents cloud reflection. Basically what this states is that what is not transferred through a layer is either reflected by or absorbed in the layer. The main problem for estimation of satellite derived SSI is to determine the effects of clouds on radiation (multiple reflection, transmission, absorption). These processes have to be related to the observed cloud albedo and the knowledge on state of the atmosphere. The methods described below illustrates various solutions to this problem.

3.1.2 CMS

This is described in several papers (e.g. Brisson et al., 1994, Brisson et al., 1999). The albedo at top of the atmosphere (A) is observed from the satellite. The first equation below relates this to Rayleigh scattering in the atmosphere (A_{ray}), the cloud albedo (A_c), the transmittance in the path Sun, Cloud, Satellite, and a term accounting for multiple scattering in the atmosphere. The cloud albedo (A_c) and transmittance (T_c) are related through a cloud factor (T_{cl}).

$$A = A_{ray} + T_{dt} A_c + \frac{A_s T_d T_c^2}{1 - T_{bc} A_s A_c}$$

$$T_c = 1 - A_c - A_c m \mu_0$$

$$T_{cl} = \frac{T_c}{1 - T_{bc} A_s A_c}$$

In the equations above T_{bc} is the atmospheric transmittance "below the cloud", A_c is the "cloud albedo", A_s is the surface albedo, T_{dt} is the transmittance in the path Sun, Cloud, Satellite and T_d similarly the transmittance Sun, Surface, Satellite, A_{ray} is the albedo due to Rayleigh scattering, and m is the cloud absorption factor.

The system of equations listed above should be solved for T_{cl}.

3.1.3 Frouin

This method is described in Frouin and Chertok (1992). The first equation below relates the satellite observed albedo (A) to the combined cloud and surface albedo (A'). The second equation describes the cloud absorption as a function of the combined albedo of the cloud and the surface and the surface albedo. By subtracting the surface albedo from the combined albedo, the cloud albedo remains. This is related to the cloud absorption through a cloud absorption factor (m). Actually, originally the relationship was made through a factor α which varied from 0.03 to 0.4 depending on

cloud liquid water content and the solar zenith angle (increasing zenith and liquid water gives decreasing α). In this implementation it is only affected by the solar zenith angle, but is confined within the limits specified. The third equation represents the cloud factor, the effect of clouds on the irradiance that reach the surface.

$$A = A_{ray} + \frac{T_{dt} A'}{1 - S_a A'}$$

$$a_c = m \mu_0 (A' - A_s)$$

$$T_{cl} = \frac{1 - A' - a_c}{1 - S_a A'}$$

In the equations above A' is the combined cloud and surface albedo, a_c is the cloud absorption, A_s is the surface albedo, T_d is the Sun−Surface−Satellite transmittance and T_{dt} is the Sun−Cloud−Satellite transmittance. A_{ray} represents the contribution of scattering in a clear atmosphere to the observed albedo. No formula is given for $A_{ray,}$ thus the formulation for Rayleigh scattering given by Brisson et al. (1999) was used. $T_{dt}A'(1-S_a a')^{-1}$ represents the contribution from multiple scattering in the cloud. S_a is the spherical albedo and accounts for multiple reflection between the surface and the cloud.

In this configuration T_{cl} in fact represents the ratio between the irradiance that reaches the surface and the irradiance that would have reached the surface under cloud free conditions, or rather if the cloud layer and surface were non reflecting and non absorbing. In other words this is the combined effect of absorption in the cloud and reflection by the cloud (and surface) on the incoming radiation. This ratio depends on the solar zenith angle.

3.1.4 Frouin & CMS

In this method the cloud factor (T_{cl}) formalism of Frouin and Chertok (1992) have been used together with the atmospheric transmittance formalism of CMS (e.g. Brisson et al., 1999).

3.2 Atmospheric transmittances

The equations given in the previous chapter requires specification of absorption due to various atmospheric constituents. The formalism used is given below. $T_?$ represents as before a transmittance, $a_?$ represents an absorption, $A_?$ an albedo, and $U_?$ an amount of absorbing matter in cm. Other variables used should be self explained in the set up of equations.

3.2.1 CMS

$$T_d = 1 - a_{O3} U_{O3} (1/\mu_0 + 1/\mu) - a_{H2O} U_{WV} (1/\mu_0 + 1/\mu) - A_{ray}(\mu_0) - A'_{ray}(\mu)$$

$$T_{dt} = 1 - a_{O3} U_{O3} (1/\mu_0 + 1/\mu) - a_{H2O} 0.3 U_{WV} (1/\mu_0 + 1/\mu) - A_{ray}(\mu_0) - A'_{ray}(\mu)$$

$$A_{ray}(\mu_0) = \frac{0.28}{1 + 6.43\mu_0}$$

where

$$T_a = \beta (1 - a_{H2O}(U_{WV}/\mu_0) - a_{O3}(U_{O3}/\mu_0) - A_{ray})$$

$$a_{H2O}(U_{WV}/\mu_0) = \frac{2.9(U_{WV}/\mu_0)}{(1 + 141.5 U_{WV}/\mu_0)^{0.635}} + 5.925 U_{WV}/\mu_0$$

$$a_{O3}(x) = a_{O3}^{VIS}(x) + a_{O3}^{UV}(x) \qquad x = U_{O3}/\mu_0$$

$$a_{O3}^{VIS}(x) = \frac{0.02118x}{1 + 0.042x + 0.000323x^2}$$

$$a_{O3}^{UV}(x) = \frac{1.082x}{(1 + 138.6x)^{0.805}} + \frac{0.0658x}{1 + (103.6x)^3}$$

$$A_{ray} = \frac{0.28}{1 + 6.43\mu_0}$$

$$\beta = e^{-0.091/\mu_0} \qquad \delta = 0.091$$

T_a above is not used as the clear sky transmittance is calculated using the Staylor parameterization (Darnell et al., 1988, Darnell et al., 1992), it is only presented for a full specification.

3.2.2 Frouin

$$\tau_d = \tau_{O3} U_{O3} (1/\mu_0 + 1/\mu) + \tau_{H2O} U_{WV} (1/\mu_0 + 1/\mu) + \tau_{sc} (1/\mu_0 + 1/\mu)$$

$$\tau_{dt} = \tau_{O3} U_{O3} (1/\mu_0 + 1/\mu) + \tau_{H2O} 0.3 U_{WV} (1/\mu_0 + 1/\mu) + \tau_{sc} (1/\mu_0 + 1/\mu)$$

$$T_d = e^{-\tau_d}$$

$$T_{dt} = e^{-\tau_{dt}}$$

where

$$T_a = \frac{e^{-\tau_{H2O}} e^{-\tau_{O3}} e^{-\tau_{sc}}}{1 - A_s(a' + b'/V)}$$

$$\tau_{H2O} = 0.102 (U_{WV}/\mu_0)^{0.29}$$

$$\tau_{O3} = 0.041 (U_{O3}/\mu_0)^{0.57}$$

$$\tau_{sc} = (a + b/V)\mu_0$$

maritime: $a = 0.059\ b = 0.359\ a' = 0.089\ b' = 0.503$

continental: $a = 0.066\ b = 0.704\ a' = 0.088\ b' = 0.456$

T_a above is not used as the clear sky transmittance is calculated using the Staylor parameterization, it is only presented for a full specification.

4 Experiment set up

4.1 Validation data

The data used for validation in this experiment was the SSI observations performed by the Geophysical Institute, University of Bergen in Bergen on the western coast of Norway and Department of Agricultural Engineering at the Agricultural University of Norway in Ås in the south−east part of Norway. Both stations are presented in Figure 1.

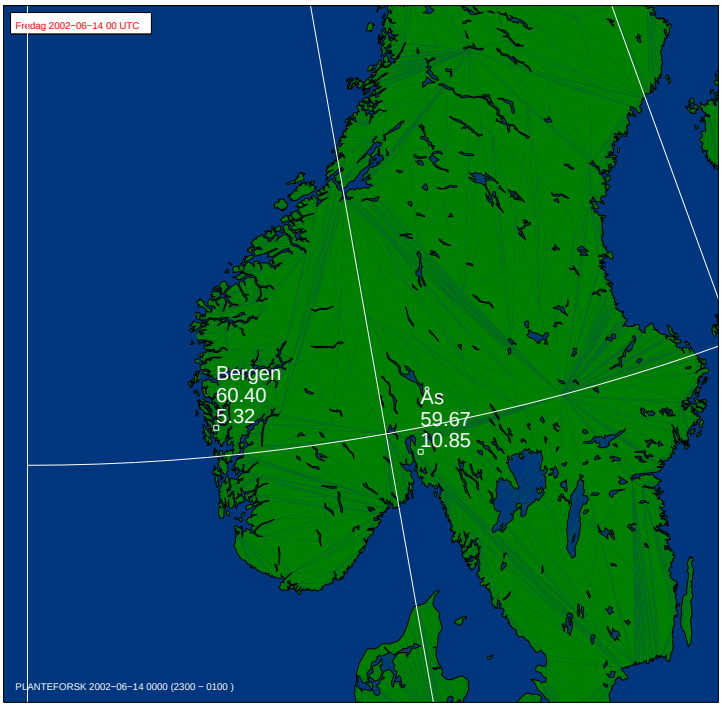

Figure 1 Validation stations used for algorithm selection.

4.2 AVHRR data

The results presented in this report have been created using two different approaches at different times in the project period. These are denoted as two different experiments, but the input AVHRR data were the same.

The AVHRR data used for this study at DNMI was processed from HRPT to level 2 by processing software delivered by Kongsberg Spacetec A/S. The level 2 data used were radiometrically and geometrically corrected and given on a Polar Stereographic map projection (correct at 60°N, no rotation) at pixel size 1.5 km. Data were output on a NCSA HDF version 4.2 format.

The first experiment set up in autumn 1999 used data spanning March − September 1999. In this experiment the AVHRR data were averaged over 10×10 pixel large boxes surrounding the validation stations and used as input to the cloud mask. The cloud covered boxes were used for SSI computations and the results were compared with validation data.

In the second experiment, performed in spring 2002 but using the same data period as in the previous experiment, the cloud mask was applied to each pixel on full resolution. Then SSI computations were performed and the results were averaged on 13×13 pixel large boxes before comparison with validation data.

4.3 Cloud mask

A very simple cloud mask using AVHRR data only was used for cloud masking in both experiments. The main features used were:

- $A2/A1 > 1$
- $T4 > 0$

No information on cloud cover were available from the validation data sets.

4.4 Atmospheric gases

For both experiments climatological values of atmospheric ozone and water vapour load were used and of surface albedo. The climatological values for Bergen was from the actual site while the data for Ås was collected for the Gardermoen airport, about 80 km further north, but in a similar landscape. However, there was one major difference between the first and second experiment. During the first experiment autumn 1999, the surface albedo used for SSI computations at Ås were the actual observed values at the station, while climatological values were used in the second experiment (making the processing similar at Ås and Bergen).

5 Results

5.1 Introduction

As mentioned above, two different set−ups have been used to evaluate the algorithms. The first experiment performed in autumn 1999 used box (10×10 pixels) averaged

AVHRR data surrounding each validation station (and observed surface albedo for NLH). No figures are provided for this experiment, but statistical values are presented in a table in Chapter 5.6. The second experiment was performed in spring 2002, using the same AVHRR data as in the first experiment, but now the algorithms were used on each individual pixel instead of on the box average. Then the flux estimates were averaged and compared to the validation data. The box size changed between the two experiments, being 10×10 in the first and 13×13 in the last. Results from this last experiment is also presented in tabular form in Chapter 5.6. In the first experiment the narrowband to broadband correction scheme was also varied along with the cloud factor algorithms. In the second experiment, the NOAA scene and cloud dependent correction was chosen and applied to all data.

The methods described in Chapter 3 were successively used with the experiment set up described in Chapter 4. Concerning the CMS method, two different cloud absorption factors were used for this method. These are specified as CMS 0.1 and CMS 0.4 in the presentation of the results for the second experiment. During the first experiment only results for a cloud absorption factor of 0.4 is presented in the table for the CMS method.

In the following chapters, illustrations for each experiment (Figure 2 − Figure 13) is provided, but no discussion on the results. This is postponed to Chapter 6. The basic illustrations provided are:

- Scatter plot of cloud covered data
- Difference plot by station for cloud covered data
- Difference plot by satellite for cloud covered data

where only fully cloud covered boxes (13×13 pixels) are used. For each pixel within a box, the cloud cover is either 0 or 1, clear or covered respectively. When creating the box value the mean cloud cover will be a value between 0 and 1 (averaged). Only boxes with fully cloud cover is used in this study. The plot type in the list above presents the scatter plot of estimated (ordinate) against observed (abscissa) values for each estimated made for both stations studied. Next the difference *observed − estimated* is presented as boxplot for each station and finally the difference for each satellite used is also presented. All statistical values presented are given for *observed − estimated*.

5.2 CMS using a cloud absorption of 0.1

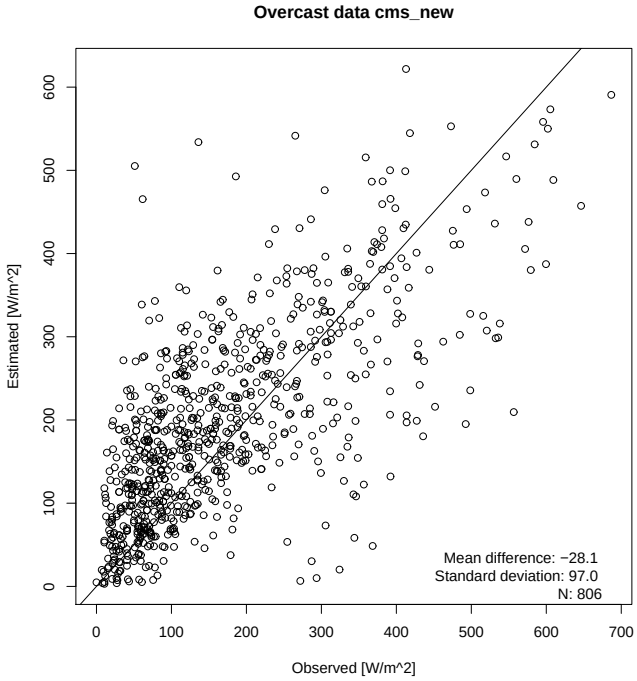

Figure 2 Scatter plot CMS method, overcast cases, cloud absorption coefficient 0.1.

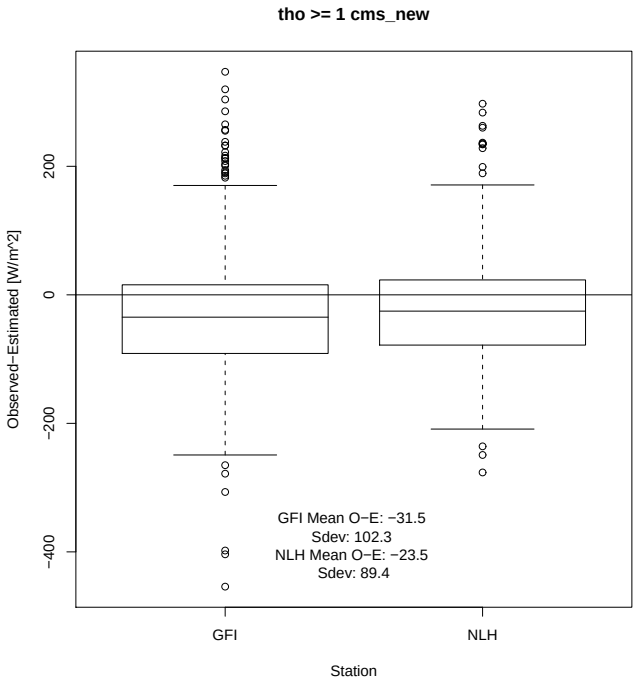

Figure 3 Difference plot by station for CMS method, overcast cases, cloud absorption coefficient 0.1

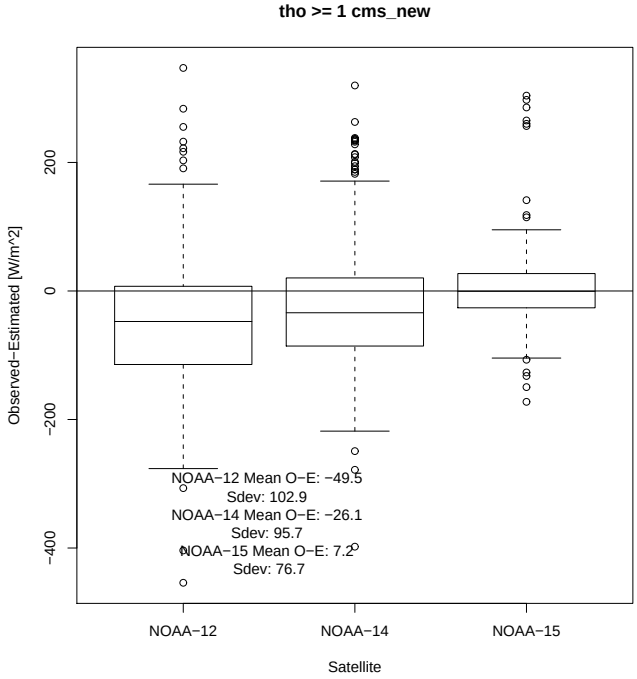

Figure 4 Difference plot by satellite CMS method, overcast cases, cloud absorption coefficient 0.1.

5.3 CMS using a cloud absorption of 0.4

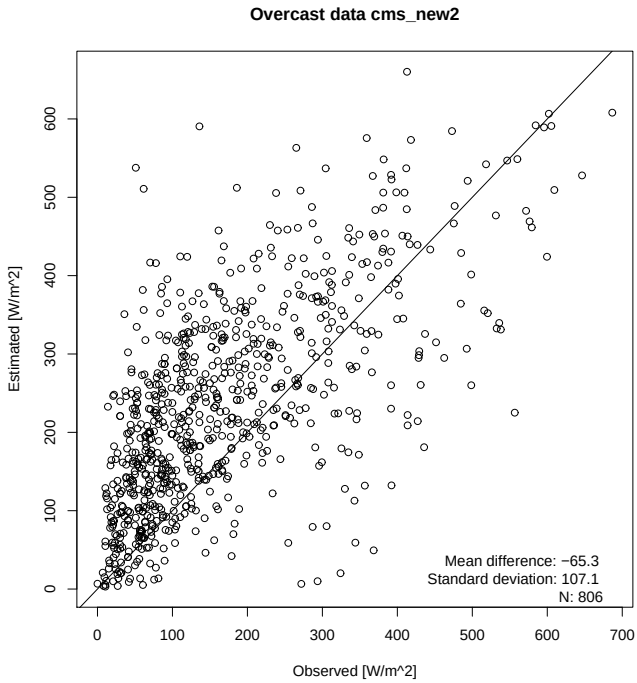

Figure 5 Scatter plot CMS method, overcast cases, cloud absorption coefficient 0.4.

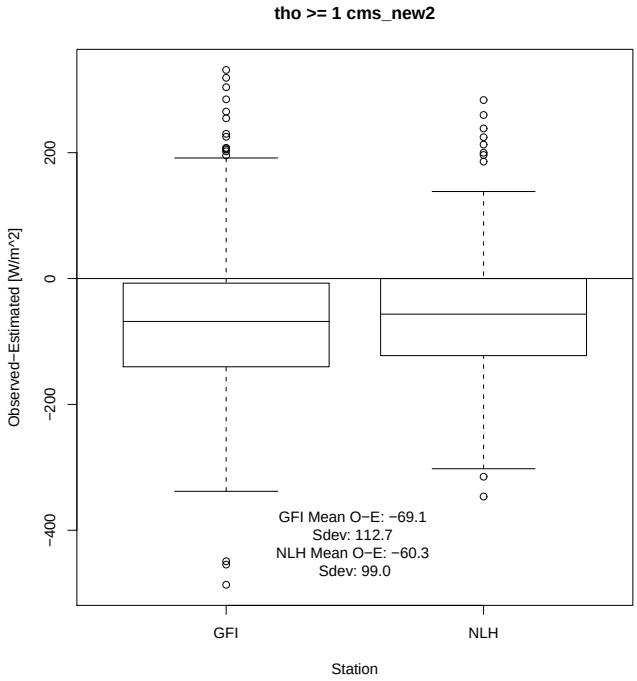

Figure 6 Difference plot by station CMS method, overcast cases, cloud absorption coefficient 0.4.

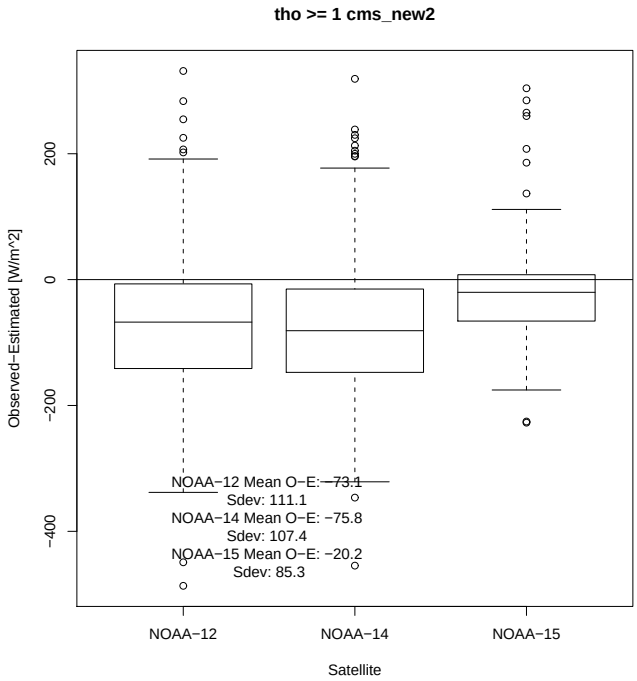

Figure 7 Difference plot by satellite − CMS method, overcast cases, cloud absorption coefficient 0.4.

5.4 Frouin

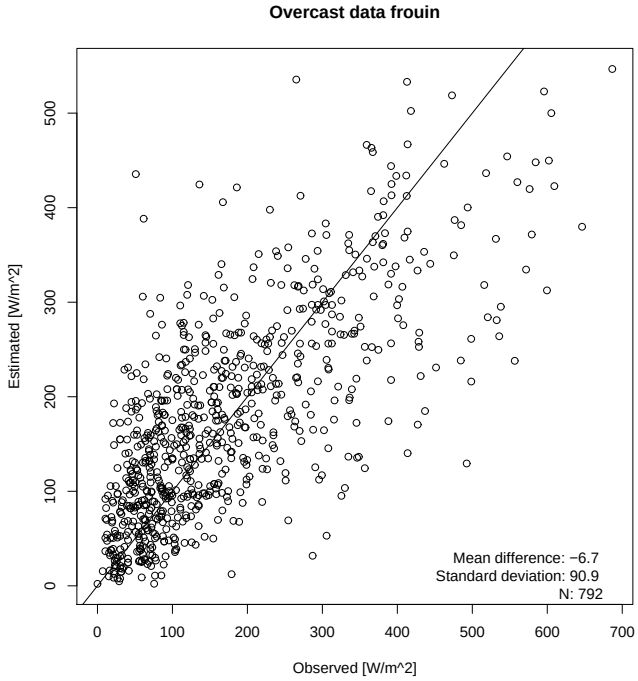

Figure 8 Scatter plot Frouin method, overcast cases.

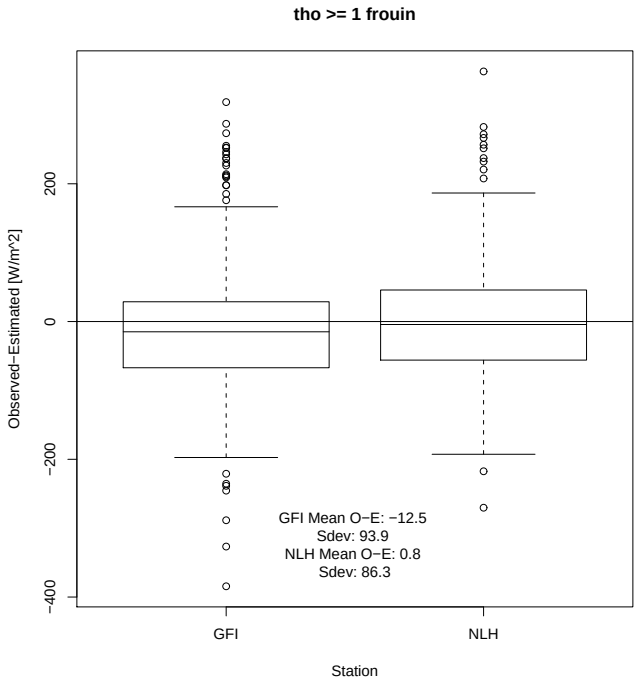

Figure 9 Difference plot by station, Frouin method, overcast cases.

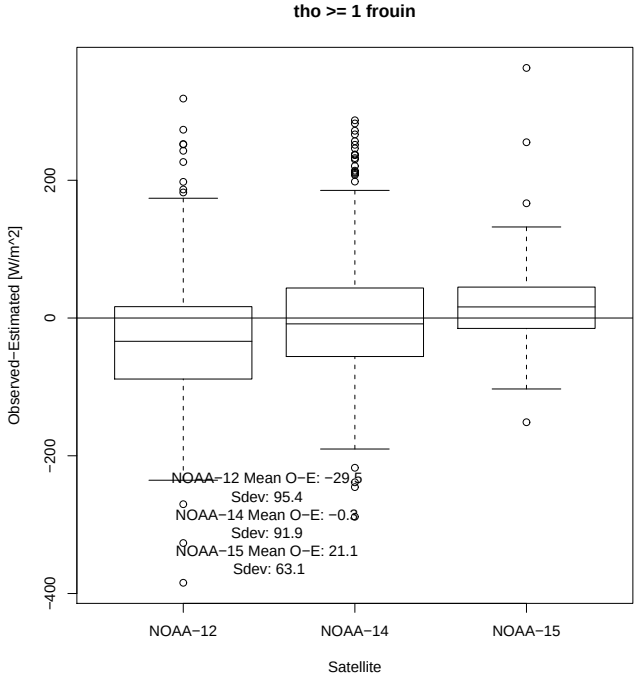

Figure 10 Difference plot by satellite Frouin method, overcast cases.

5.5 Frouin& CMS

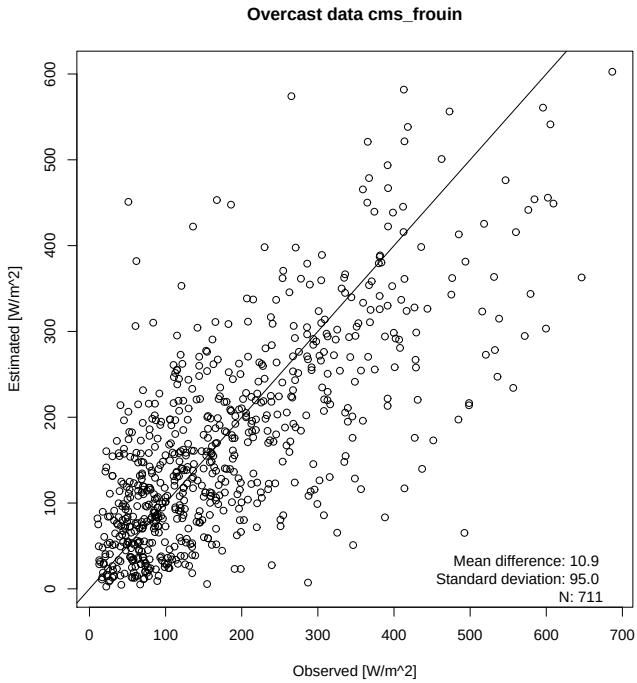

Figure 11 Scatter plot, Combined CMS & Frouin method, overcast cases.

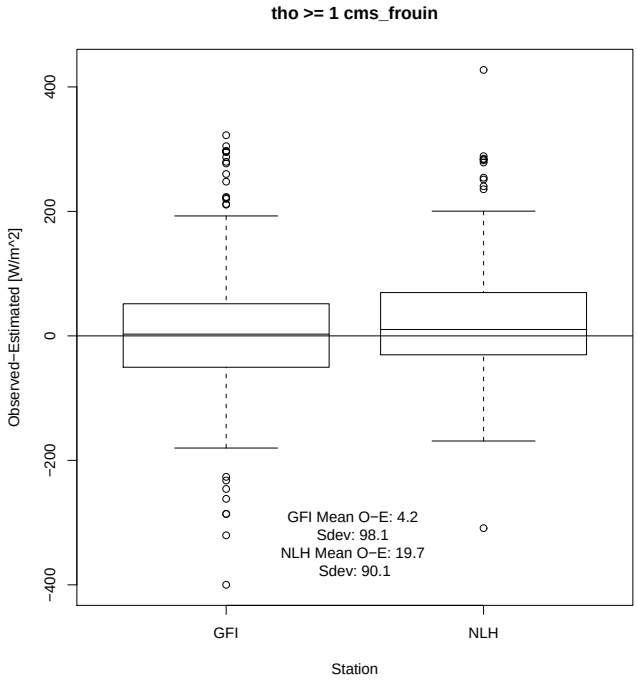

Figure 12 Difference plot by station, combined CMS & Frouin method, overcast cases.

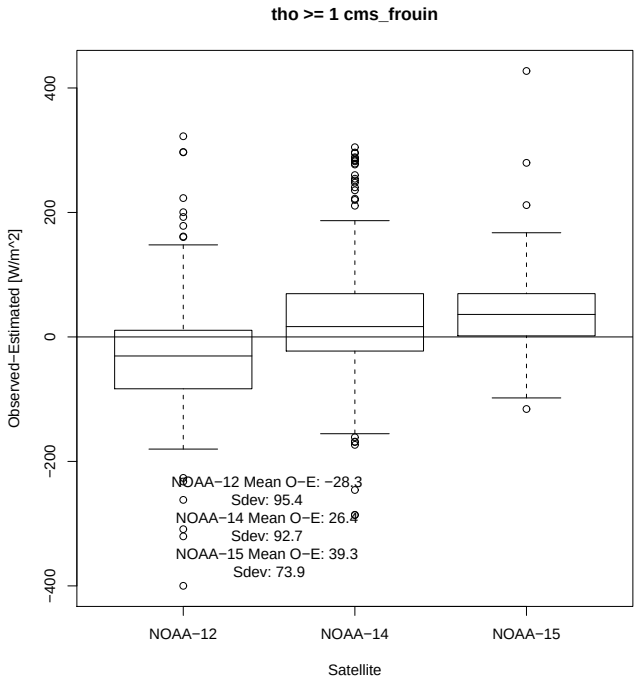

Figure 13 Difference plot by satellite, combined CMS & Frouin method, overcast cases.

5.6 Summary of statistical results

The results from comparing the algorithm estimates for cloudy conditions with real observations are presented in Figure 2 − Figure 13, and summarised in Table I and Table II.

The first experiment using averaged AVHRR data as input gave the results presented in Table I. The CMS method presented in Table I used a cloud absorption coefficient of 0.4.

The results from the second experiment testing cloudy conditions estimation of various cloud factor formalisms are presented in Table II. The two tabular presentations of results are not fully compatible. In Table I each algorithm is presented twice in combination with various NTOB correction schemes (column 2), while no such column is presented in Table II. In the second experiment it was decided to use the NOAA95 correction scheme (Godøy and Eastwood, 2002). Furthermore, as noted before the boxes used for averaging is slightly different (10×10 → 13×13). However it is not expected that the general features of the algorithm performance will change drastically due to these differences, but rather that the actual statistical values will be affected in a general way.

For further help interpreting the figures presented in the preceding chapters, the representative time identification (as given in the Kongsberg Spacetec MEOS system) is presented in Figure 14. It is seen that NOAA−12 mainly passes in the periods 06:00−08:00 UTC and 14:00−18:00 UTC, while NOAA−14 passes in 05:00−07:00 UTC and 12:00−16:00 UTC and NOAA−15 in 08:00−10:00 UTC and 16:00 − 19:00 UTC.

Table I Algorithm selection results, first experiment (1999) − cloudy data only.

Algorithm	NTOB	Bias (O−E) W/m²		Sdev W/m²	
		Bergen	Ås	Bergen	Ås
Frouin	McGill	13.15	31.38	93.37	95.63
Frouin	NOAA95	−27.91	−6.43	98.15	101.56
CMS	McGill	−24.41	−4.70	98.12	99.44
CMS	NOAA95	−69.04	−47.14	103.36	106.29
CMS+Frouin	McGill	27.83	48.57	98.50	101.63
CMS+Frouin	NOAA95	−20.08	4.82	96.63	101.13

Table II Algorithm selection results, second experiment (2002) − cloudy data only.

Algorithm	Bias Bergen	Bias Ås	Sdev Bergen	Sdev Ås
CMS 0.1	−31.5	−23.5	102.3	89.4
CMS 0.4	−69.1	−60.3	112.7	99.0
Frouin	−12.5	0.8	93.9	86.3
Frouin & CMS	4.2	19.7	98.1	90.1

6 Discussion

Studying the illustrations first, it is clearly observed that the CMS algorithm using a cloud absorption coefficient of 0.4 (Figure 5 − Figure 7) overestimates the short−wave irradiance more compared to a cloud absorption coefficient of 0.1 as used in Figure 2 − Figure 4. However, this method (for both cloud absorption coefficients) show a clear bias (overestimation), increasing with increasing irradiance in the scatter plot (Figure 2 and Figure 5). Concerning the variation with station (Figure 3 and Figure 6), it is observed that the method overestimates the irradiance more in Bergen than at Ås. Concerning variation with satellite (Figure 4 and Figure 7), best results are achieved for NOAA−15 and NOAA−14 while NOAA−12 overestimates the irradiance. This method produces the largest number of successful estimates but also the largest scatter.

The Frouin algorithm presented in Figure 8 − Figure 10, has less tendency to overestimation in the scatter plot (Figure 8) and the spread is less than for the CMS algorithm. The tendency for overestimation in Bergen compared to Ås (Figure 9) is maintained as is the satellite dependency (Figure 10) for overestimation. The number of successful estimates are about the same for this algorithm as for the CMS although a few more successful estimates were made using the CMS algorithm.

The last algorithm tested was a combination of the Frouin and CMS algorithms (Figure 11 − Figure 13) were the formalism for the cloud factor estimation was taken from the Frouin algorithm and the atmospheric transmittances were taken from the CMS algorithm. The scatter plot for this also showed quite good resemblance though the scatter (Figure 11) was slightly larger than for the pure Frouin algorithm (Figure 8) and the number of successful estimates was about 10% less than for the pure Frouin algorithm.

Concerning the differences between the first (1999) and second (2002) experiments testing the algorithms these are most readily seen from Table I and Table II. In Table I it is seen that the algorithms are tested using various versions for the narrowband to broadband (NTOB) correction. In Table II all results are achieved using the NOAA95 method. This was chosen (Godøy and Eastwood, 2002) due to the performance (number of successful computations) and underlying data source (both in time and space). The main features of Table I are found in Table II as well. In both circumstances the Frouin algorithm performs best as measured by least bias and standard deviation and highest number of successful estimates.

The results above indicates that the best fit with observed data is achieved using the Frouin parameterization (Table I and Table II). The combination of CMS double path transmittances and Frouin cloud factor formalism also gives good results for cloudy conditions. Concerning the pure CMS method this seems to be biased.

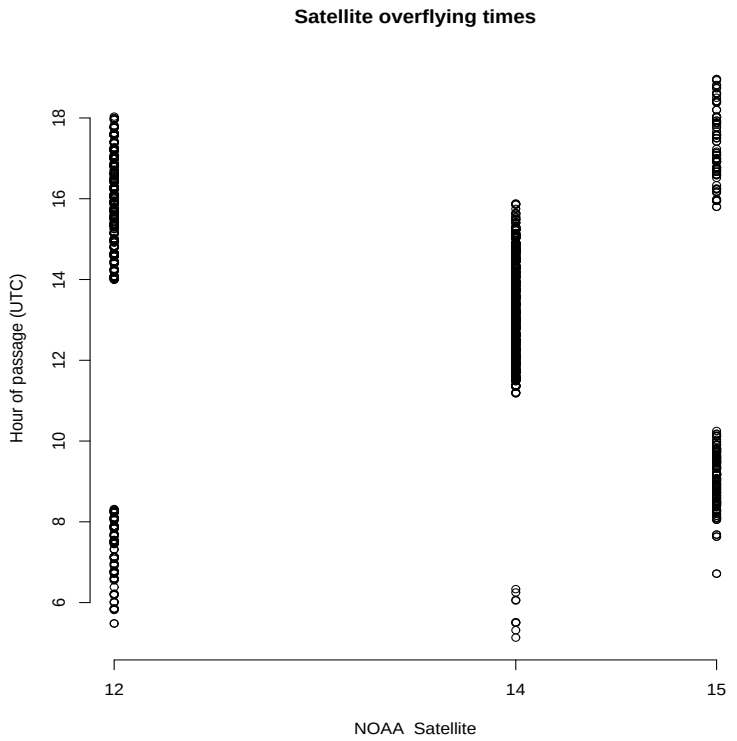

Figure 14 Passage hours of the satellites used in this study.

The results gained in this report are only for cloudy conditions, no consistency check as in Brisson et al. (1999) for the border between cloudy and clear conditions are given. Thus it is not possible to conclude on this subject. Brisson et al. (1999) concluded that the Frouin cloud factor parameterization was discontinuous and concluded that either the Staylor or the CMS parameterization could be selected along with the CMS parameterization of the double path transmittances. In the present study the CMS double path transmittances performs well also in combination with the Frouin cloud factor formalism, though a slightly larger scatter is observed. But the number of successful estimates is lowered compared to the pure Frouin method.

It is not understood why the CMS algorithm validates so poor. Several checks of the software have been performed, but no errors have been found. As the cloud absorption coefficient increases ($0.1 \rightarrow 0.4$), the cloud transmittance decreases and thus the cloud factor decreases causing the estimated irradiance to be overestimated. No other values of the cloud absorption factor have been tested due to lack of resources and control data. However, this could be advisable to check in the future concerning the results gained by Brisson et al. (1999).

Concerning the differences between the Bergen station and the Ås station, it is expected that the difference will be larger for Bergen than for Ås due to the surrounding geography. Bergen is encompassed by mountains and fiords while Ås is situated in rather flat landscape (for Norway being) surrounded by forest and agricultural land, though some ocean may influence the box sizes used for this study. However, best results for the algorithms are expected for Ås, thus the results at this station have been given priority when selecting the algorithm.

In satellite dependent illustrations presented in Chapter 5, it was observed that the

error dependency on satellite indicated that largest errors were found for NOAA−12. This a very old satellite and no compensation for sensor drift have been performed on the data. For NOAA−14 the correction proposed by NOAA (Rao and Chen, 1996, 1999) were applied and updated regularly while no compensation was performed on the NOAA−15 data. However, the NOAA−15 platform was only about a year old when this study was initiated (launched 13 may 1998). The difference between results gained using NOAA−14 and NOAA−15 is not fully understood as NOAA−14 was compensated and NOAA−15 was a quite new satellite at the time. However, if the sensor degradation of NOAA−14 was not fully corrected a decreasing albedo in time would cause an overestimation in SSI. Furthermore, as seen in Figure 14 the satellite passage times for the data used varies between NOAA−14 and NOAA−15, NOAA−15 being subject to higher solar zenith angles than NOAA−14 which may affect the quality of estimates.

Good performance on NOAA−14 / NOAA−15 and at Ås were given priority in the algorithm selection along with low scatter and a high number of successful estimates. Based upon this the Frouin algorithm was selected for use in the Ocean and Sea Ice SAF project at high latitudes.

The algorithm selection performed in this study have several drawbacks. First climatological values for atmospheric gases and surface albedo have been use, second the cloud mask is very coarse, third the consistency check between clear and cloudy cases are lacking. The first 2 objections are not supposed to alter the result significantly as they should produce similar effects for all algorithms. They may affect the error, but are not expected to change the ranking of algorithms. The consistency check is lacking and should be performed in the future when further testing of the CMS algorithm is performed as this could alter the ranking if other cloud absorption coefficients improve the CMS validation results.

7 Summary

Based upon the validation results the Frouin parameterization is chosen for the Ocean and Sea Ice SAF estimation of High Latitude surface solar irradiance using AVHRR data as input. It would be advisable to pursue the CMS parameterization further by testing various cloud absorption coefficients to achieve consistency between the GOES and POES SSI estimation and to identify any possible inconsistency between the clear and cloudy estimation process. However, at present, the Frouin method is implemented and tested for full processing of SSI and any further testing of the CMS method will be performed first on the data set from 1999, then in a parallel processing chain.

References

Brisson, A., P. Le Borgne, A. Marsouin, and T. Moreau, 1994: Surface irradiances calculated from Meteosat sensor data during SOFIA−ASTEX, Int. J. Rem. Sens., Vol. 15, No. 1, pp. 197−203, 1994.

Brisson, A., P. LeBorgne, and A. Marsouin, 1999: Development of algorithms for Surface Solar Irradiance retrieval at O&SI SAF Low and Mid Latitudes, Internal report at Météo France/SCEM/CMS, February 1999.

Darnell, W.L., F. Staylor, S.K. Gupta, and F.M. Denn, 1988: Estimation of surface insolation using sun−synchronous satellite data, J. Climate, Vol. pp. 820−835, 1988.

Darnell, W.L., W.F. Staylor, S.K. Gupta, N.A. Ritchey, and A.C. Wilbur, 1992: Seasonal variation of surface radiation budget derived from international satellite cloud climatology project C1 data, J. Geophys. Res., Vol. 97, pp. 15 741 − 15760, 1992.

Frouin, R., and B. Chertok, 1992: A Technique for Global Monitoring of Net Solar Irradiance at the Ocean Surface. Part I: Model, J. Appl. Met., Vol. 31, pp. 1056−1066.

Godøy, Ø., and S. Eastwood, 2002a: Narrowband to broadband correction of NOAA/AVHRR data, DNMI Research Note, No. 68, Norwegian Meteorological Institute, 12pp.

Godøy, Ø., 2002: Anisotropy correction for AVHRR data within the Ocean and Sea Ice SAF framework, *Report in preparation*, Norwegian Meteorological Institute.

Godøy, Ø., 2000: Evaluation of clear sky solar irradiance algorithms at high latitudes, DNMI Research Note, No. 36, Norwegian Meteorological Institute, 13pp.

Hucek, R., and H. Jacobowitz, 1995: Impact of Scene Dependence on AVHRR Albedo Models, J. Atm. Oce. Tech., Vol. 12, No. 4, pp. 697−711.

Manalo−Smith, N., G. L. Smith, S. N. Tiwari, and W. F. Staylor, 1998: Analytic forms of bi−directional reflectance functions for application to Earth radiation budget studies, J. G. R., Vol. 103, No. D16, pp. 19 733−19 751, 1998.

Paltridge, G.W., and C.M.R. Platt, 1976: Radiative processes in Meteorology and Climatology, Elsevier, ISBN 0−444−41444−4.

Rao, C.R.N, and J. Chen, 1999: Revised post−launch calibration of the visible and near−infrared channels of the Advanced Very High Resolution Radiometer (AVHRR) on the NOAA−14 spacecraft, Int. J. Rem. Sens., Vol. 20, No. 18, pp. 3485−3491.

Rao, C.N.R., and J. Chen, 1996: Post−launch calibration of the visible and near−infrared channels of the Advanced Very High Resolution Radiometer on the NOAA−14 spacecraft, Int. J. Rem. Sens., Vol. 17, pp. 2743−2747.